High-Efficiency Biwavelength Polarization Splitter-Rotator on the SOI Platform

Hang Guan, Qing Fang, Guo-Qiang Lo, and Keren Bergman

***Abstract*— We present the design of a highly efficient polarization splitter-rotator that operates at both 1310- and 1550-nm wavelength bands in a 220-nm silicon-on-insulator platform. The proposed polarization splitter-rotator has a simulated insertion loss of −0.9 dB at 1310 nm and −1 dB at 1550 nm. This is the first theoretical demonstration of a biwavelength polarization splitter-rotator. This letter is valuable for the implementation of a novel edge-coupling-based light duplexing silicon photonic system.**

***Index Terms*— Integrated optics, polarization splitter and rotator, silicon-on-insulator (SOI).**

I. Introduction

WAVELENGTH-DIVISION-MULTIPLEXED passive optical networks (WDM PONs) are regarded as a potential solution for next-generation optical access networks [1]. However, the relatively high cost of WDM PON is still one of the main limitations of its practical usage. Recently, many researchers have shifted their attention to silicon-on-insulator (SOI)-based integrated circuits that could offer a high density of integration with a relatively low cost for mass production [2], [3]. For instance, today's fiber-to-the-home (FTTH) systems usually utilize two different wavelengths for upstream and downstream traffic. Typical operational wavelengths are near 1310, 1490, or 1550 nm, which are widely spaced. Thus, one important issue of implementing WDM PON system on a SOI platform is to find an efficient mechanism to duplex light. To this end, bi-wavelength grating couplers have been proposed [4]–[7]. Xu *et al*. demonstrated a two-dimensional (2-D) bi-wavelength grating coupler with −6 dB and −6.5 dB insertion loss for 1490 and 1550 nm [5]. To further split the two orthogonal polarization states, Streshinsky *et al*. demonstrated the first bi-wavelength polarization-splitting grating coupler (PSGC) with insertion losses of −8.2 dB and −7.1 dB at 1310 nm and 1550 nm, respectively [7]. It should be noted that the above demonstration is still not ideal, since we usually prefer one polarization state rather than two orthogonal polarization states at the outputs of the grating couplers. Thus far, the design of a light coupling mechanism, which can cover two widely spaced wavelength spans, and is also insensitive to the input polarization state, remains an open question.

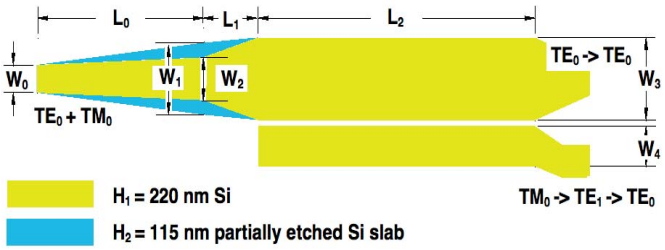

Fig. 1. Schematic of the proposed bi-wavelength PSR with significant geometric parameters noted.

In this letter, we propose a novel high-efficiency edge-coupling-based light duplexing mechanism to address this issue. Our light duplexing mechanism comprises a wide-band edge coupler and a bi-wavelength polarization splitter-rotator (PSR). The edge coupler should have a wide bandwidth that is enough to cover the two widely spaced wavelength ranges. Such low-loss and wideband edge couplers have been demonstrated in the literature [8], [9]. After light coupling, a bi-wavelength PSR is then used to split the two polarization states and rotate the TM_0 mode into the TE_0 mode. Although PSRs for single wavelength operation have been demonstrated in literature [10]–[16], bi-wavelength PSRs, which can work at two widely separated wavelengths (e.g. 240 nm) have not been demonstrated thus far. Here, we describe the first theoretical demonstration of a bi-wavelength PSR, which is designed to work in both the 1310 nm and 1550 nm bands. The PSR is composed of a wideband TM_0-to-TE_1 mode converter and an asymmetric bi-wavelength directional coupler [12]–[17]. The novelty of this letter is to show this geometry to work at two widely separated wavelength bands for the first time, which is significantly different from any previous work.

II. Principle and Simulation

The schematic of the bi-wavelength PSR is shown in Fig. 1, where the yellow regions represent the Si waveguide and the blue regions represent the partially etched slab waveguide. The Si thickness is $H_1 = 220$ nm. We choose parameter H_2 to represent the thickness of partially etched slab waveguide. This device is composed of a wideband TM_0-to-TE_1 mode

Manuscript received August 31, 2014; revised December 9, 2014; accepted December 17, 2014. Date of publication December 19, 2014; date of current version February 11, 2015.

H. Guan is with the Institute of Microelectronics, Agency for Science, Technology and Research, Singapore 138632, and also with the Department of Electrical and Computer Engineering, National University of Singapore, Singapore 119077 (e-mail: hang.guan@nus.edu.sg).

Q. Fang and G.-Q. Lo are with the Institute of Microelectronics, Agency for Science, Technology and Research, Singapore 138632 (e-mail: fangq@ime.a-star.edu.sg; logq@ime.a-star.edu.sg).

K. Bergman is with the Department of Electrical Engineering, Columbia University, New York, NY 10027 USA (e-mail: bergman@ee.columbia.edu).

Color versions of one or more of the figures in this letter are available online at http://ieeexplore.ieee.org.

Digital Object Identifier 10.1109/LPT.2014.2384451

converter, an asymmetric bi-wavelength directional coupler and a symmetric SiO_2 cladding. Both the TE_0 and TM_0 modes are launched into the left port of the bus waveguide, as shown in Fig. 1. The TE_0 mode will pass through the bus waveguide and come out from the right port of the bus waveguide directly. Meanwhile, the TM_0 mode will convert to the TE_1 mode after passing through the bi-level taper, and then couple into the access waveguide to become the TE_0 mode when passing through the asymmetric directional coupler.

However, there are two major problems that need to be solved in order for this geometry to work at two widely separated wavelengths. The first problem is how to make a bi-level TM_0-to-TE_1 converter not only highly efficient, but more importantly, very wideband. The fundamental principles of designing a highly efficient bi-level TM_0-to-TE_1 converter have been discussed in the literature [13]. However, how to design a wideband converter, which can cover two widely separated bands, has never been discussed before. In this letter, we use the particle swarm optimization (PSO) to design an ultra-wideband converter, which has a maximum TM_0-to-TE_1 mode conversion loss (MCL) of -0.2 dB in the wavelength region 1250 – 1600 nm (350 nm bandwidth). The other problem is to design a bi-wavelength asymmetric directional coupler. To be more specific, the difficulty is to size the widths of the directional coupler so that the phase-matching conditions are satisfied at two widely spaced bands.

The PSO method has been widely used in today's optical device designs to find the optimum geometries [18]–[20]. To design a low-loss and wideband bi-level taper, the geometry parameters (W_0, W_1, W_2, L_0, L_1, and H_2) need to be optimized. The other two parameters are fixed ($H_1 = 220$ nm and $W_3 = 1.25$ μm). W_3 is fixed to satisfy the phase-matching condition, which we will detail later. The optimization figure of merit (FOM) for the bi-level taper is defined as the normalized TE_1 mode power transmission at a certain wavelength, written as FOM_λ. In the optimization, we first chose 10 wavelength points across a 350 nm range (1250 – 1600 nm) and take the average of FOM_λ as FOM_{avg}. Then, we maximized FOM_{avg} to get the optimum geometry parameters for the wideband bi-level taper [19]. After optimization, we chose $W_0 = 0.40$ μm, $W_1 = 1.085$ μm, $W_2 = 0.645$ μm, $L_0 = 40$ μm, $L_1 = 4$ μm, and $H_2 = 0.115$ μm. The four parameters (W_1, W_2, H_1 and H_2) define the cross section of a rib waveguide such that the effective mode indices of the TE_1 mode and the TM_0 mode are separated widely enough at the end of the first section of the bi-level taper. The first 40-μm long taper section makes sure that the TM_0 mode and TE_1 mode acquire sufficient mode hybridization and conversion at both wavelengths. Further decreasing the length of the taper is possible, at the expense of increasing the mode conversion loss. Fig. 2(a) shows the effective mode indices of the TM_0 mode and the TE_1 mode at both wavelengths as light propagates through the bi-level taper. In the places highlighted by brown circles, strong mode hybridization and conversion occur. After traveling through the first section of the bi-level taper, the input TM_0 mode converts to the output TE_1 mode at both wavelengths. Three-dimensional finite-difference time-domain (3-D FDTD) simulation was performed to verify the MCL of this bi-level taper. Fig. 2(b) shows the simulated MCL in the wavelength regime 1250–1600 nm. The overall MCL is less than -0.2 dB.

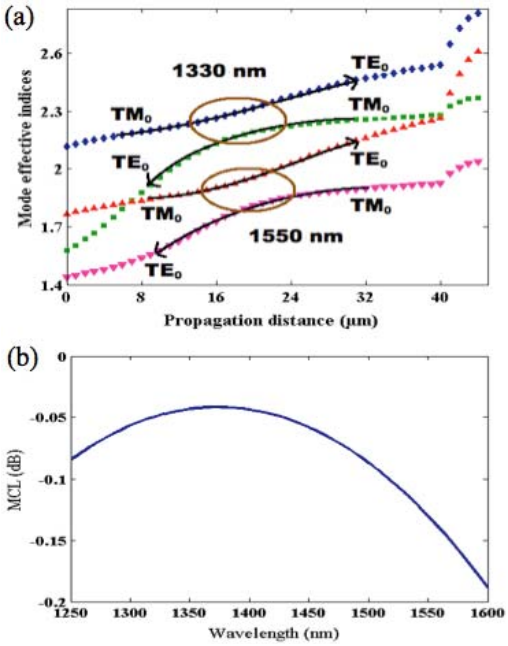

Fig. 2. (a) Mode effective indices evolution along the PSR structure. (b) Simulated MCL of the bi-level taper.

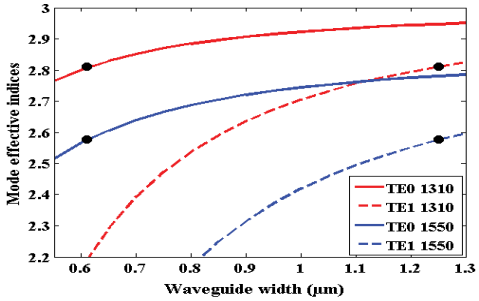

Fig. 3. Effective indices of the TE_0 mode and the TE_1 mode at 1310 nm and 1550 nm as a function of waveguide width.

The design of a bi-wavelength directional coupler comprises two steps. The first step is to choose a pair of waveguide widths so that the phase-matching conditions are satisfied at both wavelengths. Fig. 3 shows the effective indices of the TE_0 mode and the TE_1 mode at both wavelengths as a function of waveguide width. When choosing the bus waveguide width $W_3 = 1.25$ μm and the access waveguide width $W_4 = 0.61$ μm, the effective indices of the TE_1 mode in the bus waveguide are $n_{eff} = 2.577$ at 1550 nm and $n_{eff} = 2.810$ at 1310 nm. The effective indices of the TE_0 mode in the access waveguide are $n_{eff} = 2.577$ at 1550 nm and $n_{eff} = 2.808$ at 1310 nm, as marked by the four black dots in Fig. 3. So we can conclude that the phase-matching conditions for both wavelengths are simultaneously satisfied, which ensures that almost 100% power will be transferred to the other waveguide after traveling one coupling length.

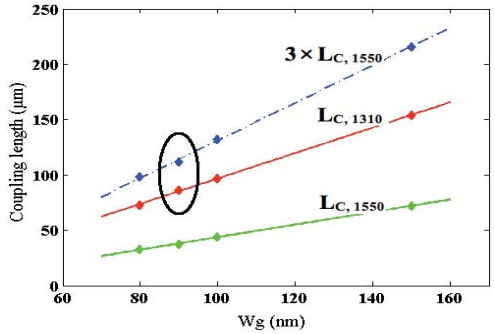

Fig. 4. $L_{C,1310}$ and $L_{C,1550}$ as a function of W_g.

The second step is to engineer the gap (W_g) so that at both wavelengths the TE_1 mode in the bus waveguide could be coupled into the TE_0 mode and come out from the access waveguide. $L_{C,1310}$ and $L_{C,1550}$ are defined as the coupling length at 1310 nm and 1550 nm, respectively. Both $L_{C,1310}$ and $L_{C,1550}$ could be treated as functions of W_g. The goal of this step to find an optimum W_g that satisfies $L_{C,1310}$ (W_g) $\approx$ n $\times$ $L_{C,1550}$ (W_g), where n is odd.

In Fig. 4, the red solid line and the green solid line show that the coupling length at both wavelengths is correlated with W_g linearly in the range between 80 nm and 150 nm. The blue dashed line shows the change of 3 $\times$ $L_{C,1550}$ with respect to W_g. To choose the optimum W_g, we need to consider a trade-off between device performance and fabrication difficulty. On one hand, we want a smaller W_g so that the maximum power locations of two wavelengths can get closer, as shown in Fig. 4. On the other hand, a smaller W_g demands higher requirements from the fabrication processes and makes it difficult to maintain high fidelity of the device [21]. For example, here we choose W_g = 90 nm, which can be patterned using electron-beam lithography and possibly using the state-of-the-art optical lithography [22].

To verify the behavior of this device, 3-D FDTD simulation was performed. Fig. 5 shows the mode profile when launching the TE_0 and TM_0 modes at both wavelengths. As can be seen from Fig. 5(b) and Fig. 5(d), the maximum power coupled into the access waveguide is located at $L_{C,1310}$ = 86 μm in 1310 nm and at 3 $\times$ $L_{C,1550}$ = 112 μm in 1550 nm. To reach a compromise, we end this directional coupler at 138 μm (L_2 = 94 μm), so that both wavelengths have high coupling efficiencies. At the end of the directional coupler, the bus waveguide is tapered back to 0.5 μm. The access waveguide is separated away from the bus waveguide by a 6 μm-long S-bend with a bend radius of 8 μm. It should be noted that the cross ports shown in Fig. 1 and Fig. 5 are actually S-bends, not polygons with sharp corners.

Fig. 6 shows the TM_0-to-TE_0 polarization conversion loss (PCL) near 1310 nm and 1550 nm. The PCL is around -1 dB for both wavelengths. It is also worth noting that the 3-dB bandwidths are wider than 50 nm in both wavelength spans, which cover most of the O-band and the entire C-band.

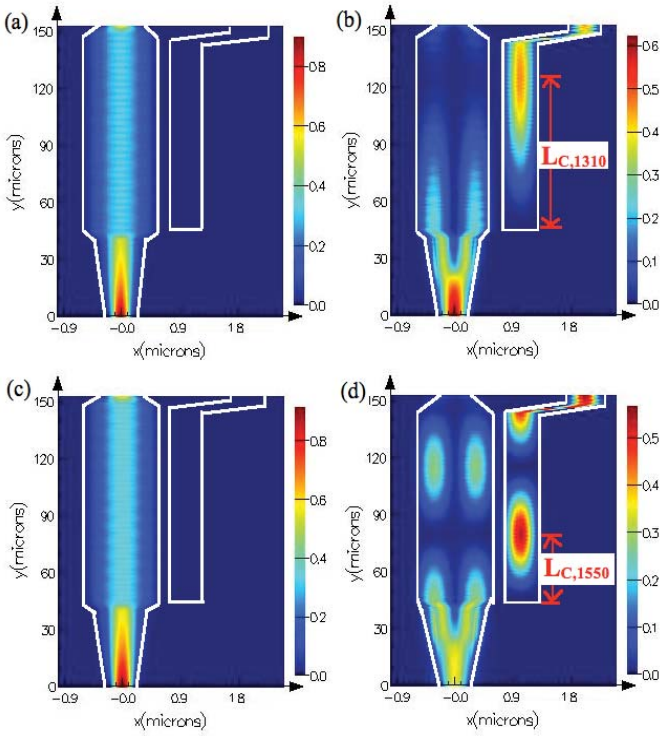

Fig. 5. Mode propagation when launching (a) TE_0 at 1310 nm, (b) TM_0 at 1310, (c) TE_0 at 1550 nm, and (d) TM_0 at 1550 nm.

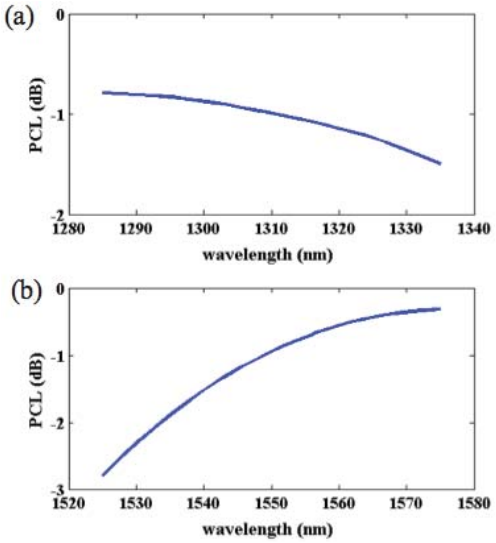

Fig. 6. Wavelength dependence of PCL centered at (a) 1310 nm, and (b) 1550 nm.

To investigate the fabrication tolerance, five key geometry parameters (W_3, W_4, W_g, H_1, and H_2) have been varied within +/− 5 nm, respectively.

As shown in Fig. 7, PCL is less sensitive to W_3, H_1 and H_2, but it is more sensitive to W_g and W_4. The PCLs at both wavelengths reach a compromise at W_g = 90 nm. The situation for W_4 is similar, as can be seen from Fig. 7(c). In reality, these parameters may have deviations at the same time, which will further degrade the PCL of this device.

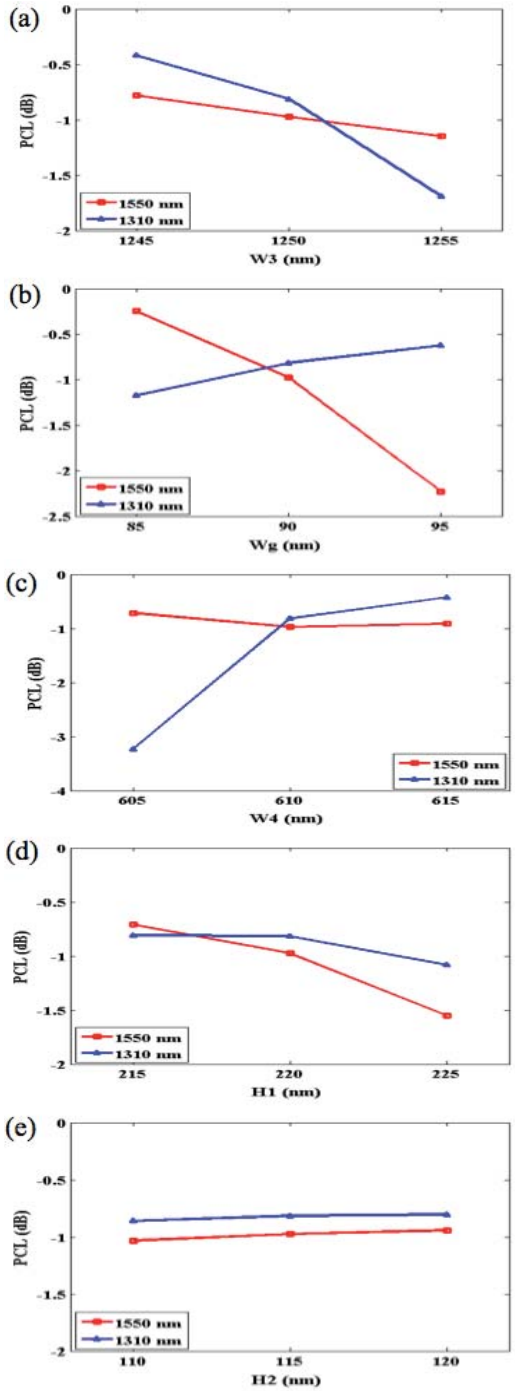

Fig. 7. PCL as a function of (a) W_3, (b) W_g, (c) W_4, (d) H_1, and (e) H_2.

Controlling these fabrication dimensions will be a challenge in achieving the low loss of 1 dB.

III. Conclusion

In conclusion, we have proposed a design methodology of bi-wavelength PSRs by utilizing a structure comprising a bi-level taper and an asymmetric directional coupler. To the best knowledge of the authors, this is the first theoretical demonstration of a bi-wavelength PSR. The proposed PSR has a simulated insertion loss of -0.9 dB at 1310 nm and -1.0 dB at 1550 nm. By adding the loss caused by the wideband edge coupler (usually < -1 dB), we have shown that this edge-coupling-based light duplexing solution is still much more efficient than the current grating-coupling-based counterparts.

References

[1] A. Banerjee *et al.*, "Wavelength-division-multiplexed passive optical network (WDM-PON) technologies for broadband access: A review [Invited]," *J. Opt. Netw.*, vol. 4, no. 11, pp. 737–758, Nov. 2005.

[2] T. Baehr-Jones, T. Pinguet, P. L. Guo-Qiang, S. Danziger, D. Prather, and M. Hochberg, "Myths and rumours of silicon photonics," *Nature Photon.*, vol. 6, pp. 206–208, Mar. 2012.

[3] M. Hochberg and T. Baehr-Jones, "Towards fabless silicon photonics," *Nature Photon.*, vol. 4, pp. 492–294, Aug. 2010.

[4] G. Roelkens, D. Vermeulen, S. Selvaraja, R. Halir, W. Bogaerts, and D. Van Thourhout, "Grating-based optical fiber interfaces for silicon-on-insulator photonic integrated circuits," *IEEE J. Sel. Topics Quantum Electron.*, vol. 17, no. 3, pp. 571–580, May/Jun. 2011.

[5] L. Xu, X. Chen, C. Li, and H. K. Tsang, "Bi-wavelength two dimensional chirped grating couplers for low cost WDM PON transceivers," *Opt. Commun.*, vol. 284, no. 8, pp. 2242–2244, Apr. 2011.

[6] W. Bogaerts, D. Taillaert, P. Dumon, E. Pluk, D. Van Thourhout, and R. Baets, "A compact polarization-independent wavelength duplexer using a polarization-diversity SOI photonic wire circuit," in *Proc. Opt. Fiber Commun. (OFC)*, Mar. 2007, pp. 1–3.

[7] M. Streshinsky *et al.*, "A compact bi-wavelength polarization splitting grating coupler fabricated in a 220 nm SOI platform," *Opt. Exp.*, vol. 21, no. 25, pp. 31019–31028, Dec. 2013.

[8] B. Ben Bakir *et al.*, "Low-loss ($<$1 dB) and polarization-insensitive edge fiber couplers fabricated on 200-mm silicon-on-insulator wafers," *IEEE Photon. Technol. Lett.*, vol. 22, no. 11, pp. 739–741, Jun. 1, 2010.

[9] Q. Fang, J. Song, X. Luo, M. Yu, G. Lo, and Y. Liu, "Mode-size converter with high coupling efficiency and broad bandwidth," *Opt. Exp.*, vol. 19, no. 22, pp. 21588–21594, Oct. 2011.

[10] L. Chen, C. R. Doerr, and Y.-K. Chen, "Compact polarization rotator on silicon for polarization-diversified circuits," *Opt. Lett.*, vol. 36, no. 4, pp. 469–471, Feb. 2011.

[11] J. Wang *et al.*, "Design of a SiO_2 top-cladding and compact polarization splitter-rotator based on a rib directional coupler," *Opt. Exp.*, vol. 22, no. 4, pp. 4137–4143, Feb. 2014.

[12] D. Dai and J. E. Bowers, "Novel concept for ultracompact polarization splitter-rotator based on silicon nanowires," *Opt. Exp.*, vol. 19, no. 11, pp. 10940–10949, May 2011.

[13] D. Dai, Y. Tang, and J. E. Bowers, "Mode conversion in tapered submicron silicon ridge optical waveguides," *Opt. Exp.*, vol. 20, no. 12, pp. 13425–13439, May 2012.

[14] Y. Ding, H. Ou, and C. Peucheret, "Wideband polarization splitter and rotator with large fabrication tolerance and simple fabrication process," *Opt. Lett.*, vol. 38, no. 8, pp. 1227–1229, Apr. 2013.

[15] W. Yuan *et al.*, "Mode-evolution-based polarization rotator-splitter design via simple fabrication process," *Opt. Exp.*, vol. 20, no. 9, pp. 10163–10169, Apr. 2012.

[16] W. D. Sacher, T. Barwicz, B. J. F. Taylor, and J. K. S. Poon, "Polarization rotator-splitters in standard active silicon photonics platforms," *Opt. Exp.*, vol. 22, no. 4, pp. 3777–3786, Feb. 2014.

[17] H. Guan *et al.*, "High-efficiency low-crosstalk 1310-nm polarization splitter and rotator," *IEEE Photon. Technol. Lett.*, vol. 26, no. 9, pp. 925–928, May 1, 2014.

[18] Y. Zhang *et al.*, "A compact and low loss Y-junction for submicron silicon waveguide," *Opt. Exp.*, vol. 21, no. 1, pp. 1310–1316, Jan. 2013.

[19] Y. Ma *et al.*, "Ultralow loss single layer submicron silicon waveguide crossing for SOI optical interconnect," *Opt. Exp.*, vol. 21, no. 24, pp. 29374–29382, Nov. 2013.

[20] H. Guan *et al.*, "Ultracompact silicon-on-insulator polarization rotator for polarization-diversified circuits," *Opt. Lett.*, vol. 39, no. 16, pp. 4703–4706, Aug. 2014.

[21] Y. Tan, R. Zhou, H. Zhang, G. Lu, and Z. Li, "Modeling and simulation of the lag effect in a deep reactive ion etching process," *J. Micromech. Microeng.*, vol. 16, no. 12, pp. 2570–2575, Oct. 2006.

[22] S. Assefa *et al.*, "A 90 nm CMOS integrated nano-photonics technology for 25 Gbps WDM optical communications applications," in *Proc. IEEE Int. Electron Devices Meeting (IEDM)*, Dec. 2012, pp. 33.8.1–33.8.3.